Paracrystalline structure of activated carbons

2001 J. Phys.: Condens. Matter 13 5545

(http://iopscience.iop.org/0953-8984/13/24/301)

INSTITUTE OF PHYSICS PUBLISHING JOURNAL OF PHYSICS: CONDENSED MATTER

J. Phys.: Condens. Matter **13** (2001) 5545–5561 www.iop.org/Journals/cm PII: S0953-8984(01)19862-0

Paracrystalline structure of activated carbons

A Szczygielska[1], **A Burian**[1] **and J C Dore**[2]

[1] Institute of Physics, University of Silesia, ulica Uniwersytecka 4, 40-007 Katowice, Poland
[2] School of Physical Science, University of Kent, Canterbury CT2 7NR, UK

Received 7 December 2000, in final form 11 April 2001

Abstract

Structural studies by means of neutron diffraction of activated carbons, prepared from a polymer of phenol formaldehyde resin by carbonization and activation processes, with variable porosity, are presented. The neutron scattering data were recorded over the range of the scattering vector $\boldsymbol{Q}$ from 2.5 to 500 nm^{-1}. The structure of activated carbons has been described in terms of disordered graphite-like layers with very weak interlayer correlations. The model has been generated by computer simulations and its validity has been tested by comparison of the experimental and calculated intensity functions. Modelling studies have shown that the model containing 3–4 layers each about 2 nm in diameter accounts for the experimental data and that graphite layers are randomly translated and rotated, according to the turbostratic structure. Near-neighbour carbon–carbon distances of about 0.139 nm and 0.154 nm have been determined. The Debye–Waller factor $\exp(-Q^2\sigma^2/2)$ with $\sigma = \sigma_0\sqrt{r}$ suggests a paracrystalline structure within a single layer. The value of the interlayer spacing of 0.36 nm has been found from paracrystalline simulations of the layer arrangement in the c-axis direction. The high quality of the experimental data has enabled determination of the coordination numbers, the interatomic distances and their standard deviations using a curve-fitting procedure over the $\boldsymbol{Q}$-range from 250 nm to 500 nm, providing structural information about short- and intermediate-range ordering.

1. Introduction

Activated carbons are a class of carbonaceous materials with a very large internal surface area and therefore they are used in a great number of applications in the chemical, pharmaceutical, food-processing and other industries [1], to dechlorinate, decolourize, purify (e.g. the filtration of wines, spirits and beers, to improve colour and flavour) and as catalyst supports in oxidation, combination, decomposition and elimination reactions [2, 3]. These materials are usually prepared by carbonization and activation of organic precursors such a phenolic resin, cellulose, saccharose and natural products such as olive or peach stones. The atomic-scale structure of these materials has been the subject of numerous x-ray, electron and neutron diffraction studies and electron microscopy observations. Although porous activated carbons have been known

of for a long time and have great commercial importance, their structure at the atomic level is not fully understood.

Diffraction methods yield a fully statistical description of disordered samples based on an analysis of the diffraction profiles. The structural information about the atomic arrangement in two-dimensional layers and their stacking can be obtained either by the Fourier analysis of well resolved peaks or from modelling studies. The first approach to the structure of activated carbons, the so-called turbostratic model, was offered by Warren [4]. In such a model the perfect graphite layers are stacked without spatial corrections. Warren derived the analytical formula for the scattered intensity [4, 5], assuming disorder in the layer stacking. Then this approach was developed by Kodera, Minami and Ino and applied to glassy carbons [6]. Mildner and Carpenter [7] performed an analysis in real space, calculating the contribution to the radial distribution function (RDF) resulting from the turbostratic structure with one interlayer spacing. Analysing models of different sizes, based on the graphite structure, Alvarez and Dore [8] suggested that a model composed of three to four layers can account for the experimental data in the case of different carbons prepared from organic precursors. Additionally these authors showed that when the size of the layer exceeds 2 nm the layer shape has no effect on the single-layer diffraction pattern. Analysing the x-ray scattering data for glassy carbon produced from a polymer of furfuryl alcohol, Ergun and Schehl [9] showed that a model based on the quinoid structure can satisfactorily account for experimental RDF data. These findings are in agreement with Pauling's earlier suggestion [10] that properties of graphitic materials can be explained by a structure in which the double bonds between adjacent carbon atoms in a single graphitic layer do not resonate equally among all of the positions, but instead are concentrated to a large extent at certain positions. Recently Burian *et al* [11] and Dore *et al* [12] reported that the turbostratic model consisting of four layers with paracrystalline distortion of the hexagonal network within a single layer reproduces very well all features of the experimental RDFs. Because the RDF is only weakly sensitive to the number of layers, we propose in this paper a different approach to the structure of activated carbons, prepared from phenolic resin, which is based on analysis of the experimental data in reciprocal space.

The activated carbons were obtained from a polymer of phenol formaldehyde resin by carbonization in nitrogen flow at 1273 K and then activated with carbon dioxide at 1073 K for varying time periods. The degrees of activation, increasing with the time period, measured as 'burn-off'—that is, the percentage weight loss—are 0%, 14% and 32%. In the present paper the results for the sample with 32% 'burn-off' are reported, because there are practically no differences in intensity within the 5% precision of the method between the samples with 0%, 14% and 32% 'burn-off' as shown in [11], and the results of simulations look very similar for the remaining samples. The differences are visible only in the small-angle region, in which the contribution to the intensity is due to the scattering coming from the pores created in the samples during the preparation and thermal treatment processes [11]. The Cartesian coordinates of the atoms have been generated by a series of computer simulations and the model intensity functions have been calculated using Debye's equation with the Debye–Waller damping term. In the case of strongly disordered materials, it is recommended that the results of model simulations are compared with the experimental data in both real and reciprocal space in order to account for all features of the structure, which can have different effects on the intensity and radial distribution function.

2. Theoretical background

The neutron scattering data were collected using the Liquids and Amorphous Materials Diffractometer (LAD) at the ISIS pulsed neutron facility of the Rutherford Appleton Laboratory

(UK) and are described in detail in [11, 12].

The samples studied in this work are partially disordered and their structure is, through as assembly of ordered regions, randomly distributed in space. In the case of scattering by a disordered system, the intensity distribution, averaged over all orientations, can be described by Debye's equation as follows:

$$I_N(Q) = b^2 \left\langle \sum_{i=1}^{N} \sum_{j=1}^{N} \mathrm{e}^{-\mathrm{i}(\boldsymbol{Q}\cdot\boldsymbol{r}_{ij})} \right\rangle_{\text{all orientations}} = b^2 \sum_{i=1}^{N} \sum_{j=1}^{N} \frac{\sin Qr_{ij}}{Qr_{ij}} \tag{1}$$

where: $Q = 4\pi(\sin\theta)/\lambda$ is the scattering vector; 2θ is the scattering angle; λ is the wavelength; N indicates the number of atoms; b is the coherent scattering length of carbon; and r_{ij} denotes the distance between the ith and jth atoms.

For the modelling of the structure of the activated carbons, Debye's equation, normalized to one atom, was used. Attenuation of the intensity due to structural disorder (thermal vibration of atoms and static disorder) is taken into account by including a Debye–Waller-type term and finally the intensity per atom is given by

$$I(Q) = b^2 \frac{1}{N} \sum_{i=1}^{N} \sum_{j=1}^{N} \frac{\sin Qr_{ij}}{Qr_{ij}} \exp\left(-\frac{\sigma_{ij}^2 Q^2}{2}\right). \tag{2}$$

The first diffraction peak, appearing at about 16 nm^{-1}, contains information about the interlayer spacing, its spread and the number of graphite layers in the samples. However, it has practically no influence on the RDF as can be seen from inspection of figure 1 in which the reduced RDF functions, computed over the Q-ranges of 0–500 nm^{-1} and 25–500 nm^{-1}, are shown. The reduced RDF function is expressed as a Fourier transform of the corrected and normalized intensity $I(Q)$:

$$d(r) = \frac{2}{\pi} \int_{Q_{\min}}^{Q_{\max}} Q \frac{I(Q) - b^2}{b^2} \sin Qr \, \mathrm{d}Q \tag{3}$$

where $Q_{\min}$ and $Q_{\max}$ indicate the range of the scattering vector values taken for computation of the RDF. Comparison of the curves shown in figure 1 clearly shows that in order to learn more about the layer stacking, structure analysis of the data in reciprocal space is necessary.

In the modelling studies presented in this work, the intensity of neutrons scattered by atoms arranged according to the graphite structure is calculated using the Debye equation and then disorder is imposed on such a structure. The unwanted small-angle component, which represents the Debye volume scattering is reduced using the method proposed by Mitchell [13]. The model is defined by the radius of the ordered region, the number of layers in the stack, the values of the lattice parameters of graphite and the standard deviations of the interatomic distances for atoms lying in the same layer (σ_{intra}) and in different layers (σ_{inter}). The computation routine allows one to vary the values of the graphite lattice constants a, c and the σ-parameters for different atomic pairs. The generalized Debye–Waller factor with $\sigma_{intra} = \sigma_0\sqrt{r}$ and $\sigma_{inter} = \sigma_1\sqrt{\Delta n}$, where $\Delta n = n_i - n_j$ (n_i and n_j label the layer positions in a sequence) can be included assuming σ_0 and σ_1 as the adjustable parameters. Such a form of σ results from the paracrystalline theory developed by Hosemann and his group [14]. The paracrystalline model is based on the assumption that the distances from any atom to adjacent atoms fluctuate without statistical correlations and that these fluctuations propagate proportionally to the square root of the interatomic distance according to the combination law of independent probability distributions of the Gaussian type. The paracrystalline theory [15, 16] implies the so-called 'α^*-relation' which is expressed as

$$\sqrt{N}g = \alpha^* \tag{4}$$

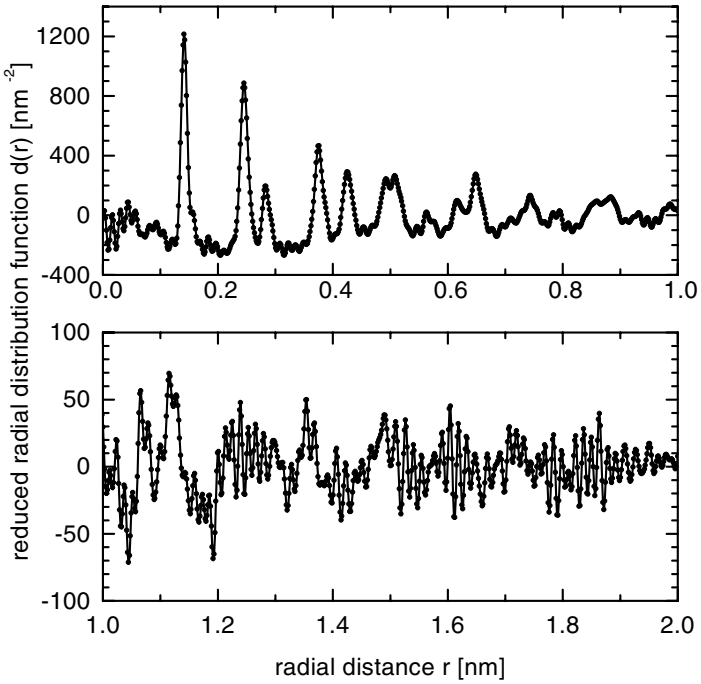

Figure 1. Reduced radial distribution functions calculated for two different Q-ranges, namely 0–500 nm^{-1} (solid line) and 25–500 nm^{-1} (full circles), respectively.

where $0.15 \leqslant \alpha^* \leqslant 0.20$, N indicates the average number of the net-planes in the paracrystal,

$$g = \sqrt{\frac{\langle d^2 \rangle - \langle d \rangle^2}{\langle d \rangle^2}}$$

is the relative statistical deviation of the interplanar spacing d in the paracrystal, d is the interplanar distance for the net-planes with the highest density of atoms and $\langle\ \rangle$ indicates the statistical average value of the quantity in the brackets. The relation given by equation (4) has the physical meaning that real paracrystals have limited sizes controlled by a degree of disorder indicated by g and that the surface net-planes have a statistical roughness of 0.15–0.20 of the net-plane distance. In other words, large paracrystals are not strongly distorted. Additionally the paracrystalline structure in the c-axis direction is simulated. This kind of defective one-dimensional lattice is generated by computer simulations with Gaussian distribution of the interlayer spacing. In order to obtain a good statistical representation of the normal distribution, the intensity function is calculated many times and then averaged. The routine employed to generate a series of random numbers with the Gaussian distribution is based on the central-limit theorem [17]. First the random variable X' with a Gaussian distribution and the mean value 0 and the variance 1 is generated according to

$$X' = \left(\sum_{i=1}^{n} X_i - \frac{n}{2} \right) \Big/ \sqrt{\frac{n}{12}} \tag{5}$$

where X_i is the random variable with uniform distribution over the (0, 1) range. The values of the translation vectors X'', which are the random Gaussian numbers with the mean value μ

and the standard deviation σ, are obtained as

$$X'' = X'\sigma + \mu. \tag{6}$$

Moreover, in the next stage of modelling, the graphite layers can be randomly translated or rotated in a limited interval according to the turbostratic model introduced by Warren [4]. The atomic coordinates defined by the model with different types and degrees of disorder are used to calculate the interatomic distances and the coordination numbers and then to compute the intensity function.

3. Results

3.1. Modelling studies

The scattered intensities for the three samples investigated were corrected for background, container and multiple scattering and then normalized using standard procedures [18]. The resulting normalized intensity functions for all samples investigated were presented in our earlier papers [11, 12]. The computation procedure consists of three main steps. The first program creates the file with the Cartesian coordinates of atoms arranged according to the graphite symmetry and the σ-parameters. In the next step, the interatomic distances and the coordination numbers are computed and a σ-value is assigned to each distance, appropriately to an assumed disorder. These data constitute the input file for the third program, which calculates the intensity function. The intermediate step reduces the computing time appreciably because the terms in equation (2), containing the same interatomic distances r_{ij}, are not calculated for each atomic pair; instead they are accumulated and then multiplied by the appropriate coordination number.

In the present work scattered neutrons were detected by a set of 14 independent and fixed-angle detectors (seven pairs of detectors symmetically mounted on each side of the instrument). The relative resolution $\Delta Q/Q$ varied from 11% for the forward angle (the scattering angle of 5°) to 0.5% for the backward angle (the scattering angle of 150°) [18]. The resolution, especially at the backward-angle detectors, is comparable to what is achieved by good powder diffractometers. The data recorded in the different detector banks were then combined to cover the Q-range from about 5 nm^{-1} to 500 nm^{-1}. The resolution ΔQ for the resulting intensities varied from 1.1 nm^{-1} in the low-Q region (10–30 nm^{-1}) to 2.5 nm^{-1} at $Q = 500$ nm^{-1}. The estimated full widths at half-maximum (FWHM) of the diffraction peaks change from about 9 nm $^{-1}$ to 2.5 nm^{-1} in the low- and high-Q ranges, respectively. The FWHMs indicate that the samples investigated exhibit a significant degree of disorder and the recorded diffraction patterns are of a rather amorphous type. Comparison of the estimated FWHMs and the instrumental resolution shows that the former does not produce a significant effect on the present analysis because it is of 10–12% of the measured diffraction peak widths.

First attempts were made to simulate the experimental intensity $I(Q)$ using micro-crystalline models with the graphite structure. The intensity function for the models with the perfect graphite structure, and with the values of the lattice constants $a = 0.2456$ nm and $c = 0.6696$ nm, containing eight, four, three and two layers with standard deviation of the interatomic distances for atoms lying in the same and in different layers $\sigma_{intra} = \sigma_{inter} = 0.005$ nm, were calculated. The radius of the ordered region within a single layer was assumed to be 1 nm. The results are compared with the experimental $I(Q)$ function in figure 2. This comparison shows that generally the calculated functions exhibit more structure, even in the case of a model consisting of two layers, for which the diffraction maxima have much higher

amplitudes than those observed experimentally beyond 80 nm^{-1}. The overall shape of the experimental functions is very similar to that for turbostratic structure [4–7, 9] where only (00l) and (hk0) diffraction lines are observed. The absence of the general (hkl) reflections is an indication of weakening in the –ABAB– graphite correlations. Nevertheless, the results of this microcrystalline modelling are given in the present paper to emphasize the dependence of the diffraction pattern on the number of layers in ordered regions and the effect of disorder on the peak amplitudes. From inspection of figure 2, it can be seen that the size of the ordered regions is limited in the c-axis direction and therefore models composed of no more than 3–4 layers will be considered for further simulations. Moreover, a shift of the first peak of the calculated function towards a higher Q-value is observed, indicating that the interplanar spacing in the carbons investigated is greater than that of graphite. This is in agreement with the Alvarez and Dore findings that only a few ($\sim$4) layers are compatible with the observed diffraction patterns for most non-graphitizing activated carbons [8]. From the comparison shown in figure 2, one can conclude that the model of the perfect graphite structure, distorted

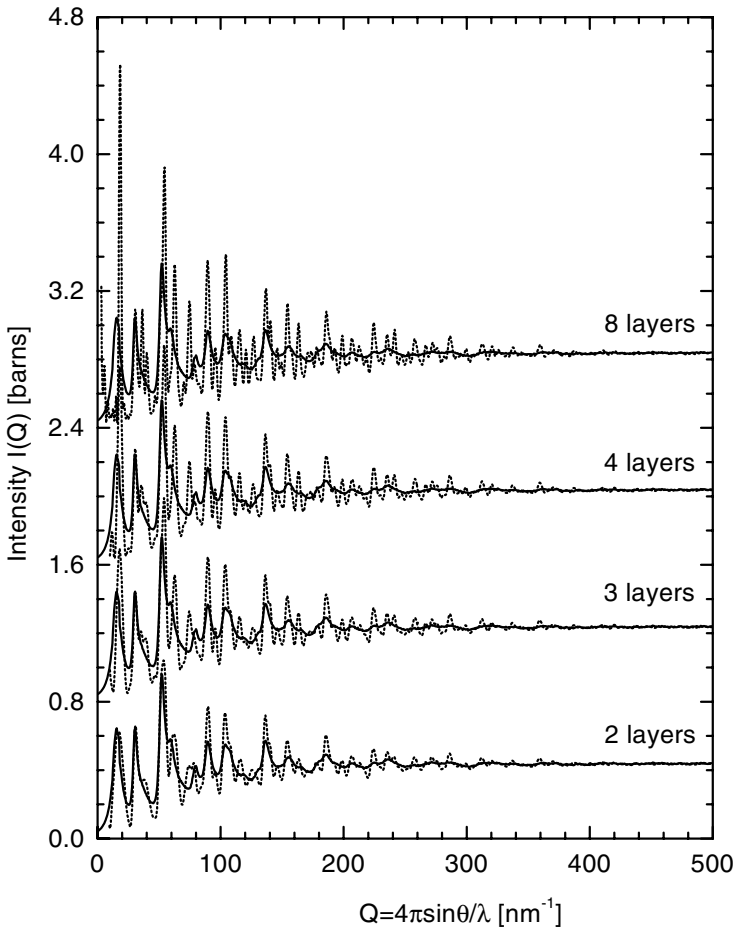

Figure 2. Comparison of the experimental (solid line) and simulated (dotted line) intensity functions for the graphite-type structure containing two, three, four and eight layers. The σ-values for atoms lying in the same and in different layers are equal: $\sigma_{intra} = \sigma_{inter} = 0.005$ nm.

only by random displacement of the atoms from the equilibrium positions with the standard deviation $\sigma_{intra} = \sigma_{inter} = 0.005$ nm, cannot explain the experimental observations. Thus weakening of the interlayer correlations is necessary to reproduce the experimental functions.

In order to attenuate the interlayer correlations, the value of the standard deviation $\sigma_{inter} = 0.025$ nm was chosen for atoms situated in different layers. The results of such simulations for three and four layers are shown in figure 3. It can be seen that this additional attenuation is not sufficient to explain disorder in an atomic arrangement in the carbon investigated. Although the greater σ_{inter} (standard deviation for atoms lying in different layers) leads to an overall attenuation of the calculated intensity function and reduces the number of peaks, agreement with the experimental function is not satisfactory. All the peaks of the calculated function for a model containing four layers are much higher than those observed experimentally. The peak amplitudes of the intensity function calculated with the model with three layers are smaller but not enough to fit the experimental function. From this comparison it can be concluded that the model in which the interlayer correlations are attenuated by the relatively high σ_{inter}-value for the atoms situated in different layers does not account for the experimental data. Additionally, it is important to point out that the amplitudes of the peaks in the experimental intensity function decrease and that their widths increase with Q. This feature cannot be explained by a simple model with disorder of the thermal vibration type. In fact, it is impossible to attenuate the peak amplitudes over the whole range of Q-values assuming a simple Debye–Waller factor. As stated above, increase in the widths of the peaks with Q is not significantly affected by the instrument resolution.

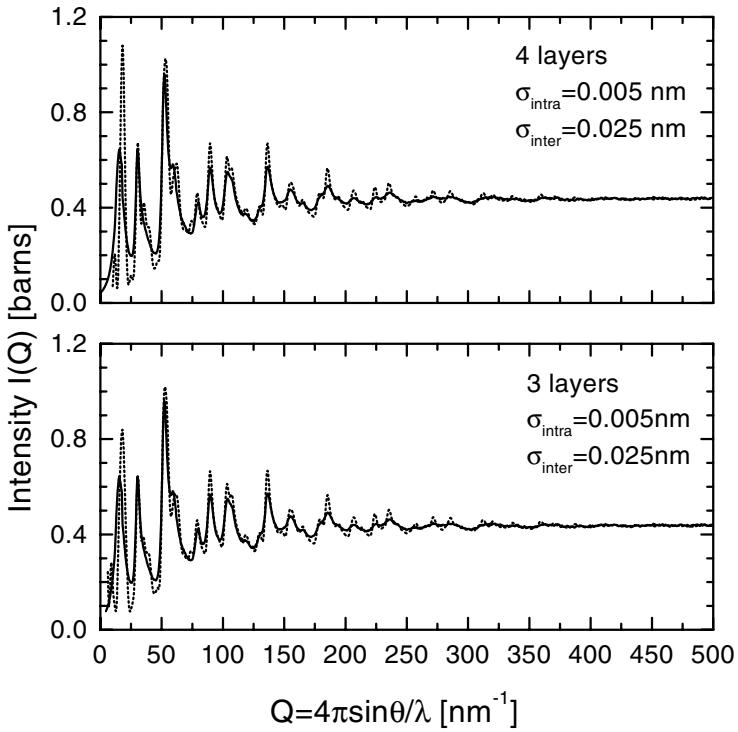

Figure 3. Experimental intensity functions (solid line) and intensity functions calculated with the model consisting of three and four layers with standard deviations $\sigma_{intra} = 0.005$ nm and $\sigma_{inter} = 0.025$ nm (dotted line).

In the next step of the modelling, the paracrystalline theory was applied. The paracrystalline distortion is introduced assuming standard deviations of the interatomic distances between atoms lying in one layer ($\sigma_{intra} = \sigma_0\sqrt{r}$) and in different layers ($\sigma_{inter} = \sigma_1\sqrt{\Delta n}$) with σ_0, σ_1 as adjustable parameters. The result of such a simulation for a model consisting of three layers with $\sigma_0 = 0.00462$ nm and $\sigma_1 = 0.015$ nm is shown in figure 4. The agreement between the experimental and simulated function presented in figure 4 is generally good. Beyond 70 nm^{-1} all features of the experimental function can be reproduced using the model with paracrystalline structure within a single layer. This kind of disorder causes increase in σ with $\sqrt{r}$ and leads to a loss of long-range ordering. This model explains the broadening of the diffraction peaks which increase with Q^2 according to [14–16]. At this stage of the modelling it is essential to point out that the paracrystalline model describes the structure of the carbons investigated reasonably well; nevertheless, some phase shift between the model and experimental function can be seen in the bottom part of figure 4 in the Q-range from 250 to 500 nm^{-1}.

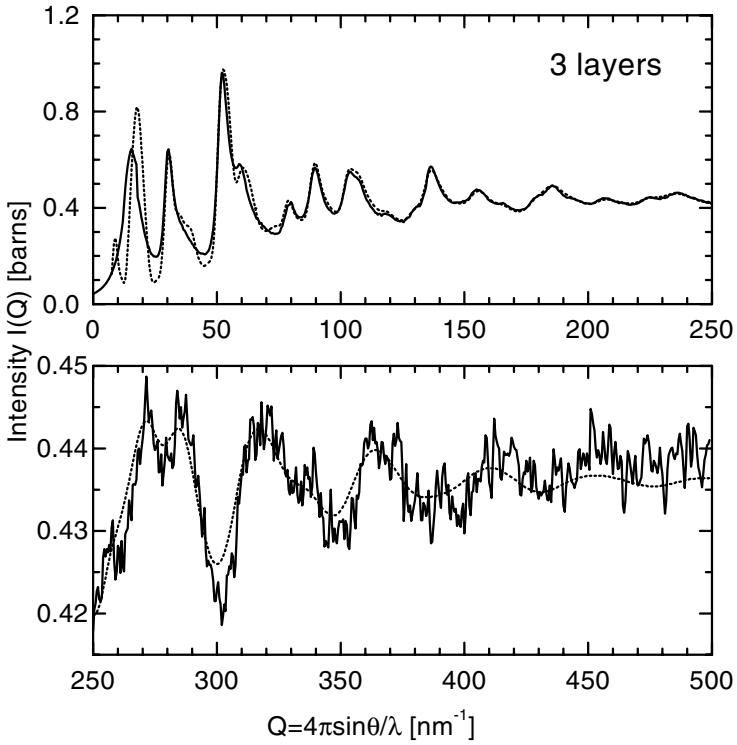

Figure 4. Experimental intensity functions (solid line) and intensity functions calculated with the paracrystalline model consisting of three layers with $\sigma_{inter} = 0.00462\sqrt{r}$ nm and $\sigma_{inter} = 0.025$ nm (dotted line).

The first diffraction peak (the (002) peak in graphite) corresponds to the interplane spacing ($c/2$). The third peak (004) observed at about 38 nm^{-1}, corresponding to twice the interplanar spacing, is more spread out and is not well separated from the (100) one. This suggests that the carbons investigated have more distorted interlayer stacking. The diffraction peaks which are shown in figure 4 are asymmetrical on the high-Q side. This kind of asymmetry is connected with the turbostratic model of carbon [4, 9]. Therefore, in the next step, the

turbostratic structure with paracrystalline stacking of layers was simulated. Starting from the graphite arrangement of atoms, the turbostratic structure with random translations or rotations of layers was generated. Models containing three layers were considered. The translation vectors, lying in the plane of a layer, were assumed to be random numbers with uniform distribution over the $(-a/2, a/2)$ and $(-a/4, a/4)$ ranges. The random rotations of successive layers were achieved by generation of the rotation angle φ as a random number with uniform distribution over the $(-\pi/2, \pi/2)$ and $(-\pi/4, \pi/4)$ ranges. In figure 5 the comparison of four different calculated intensity functions with the rotation angles and the translation vectors from the $(-\pi/4, \pi/4)$, $(-\pi/2, \pi/2)$ and $(-a/4, a/4)$, $(-a/2, a/2)$ ranges, respectively, in the Q-region from 0 to 100 nm^{-1} is shown. Beyond the 100 nm^{-1} limit all functions are practically indistinguishable within the thickness of the line.

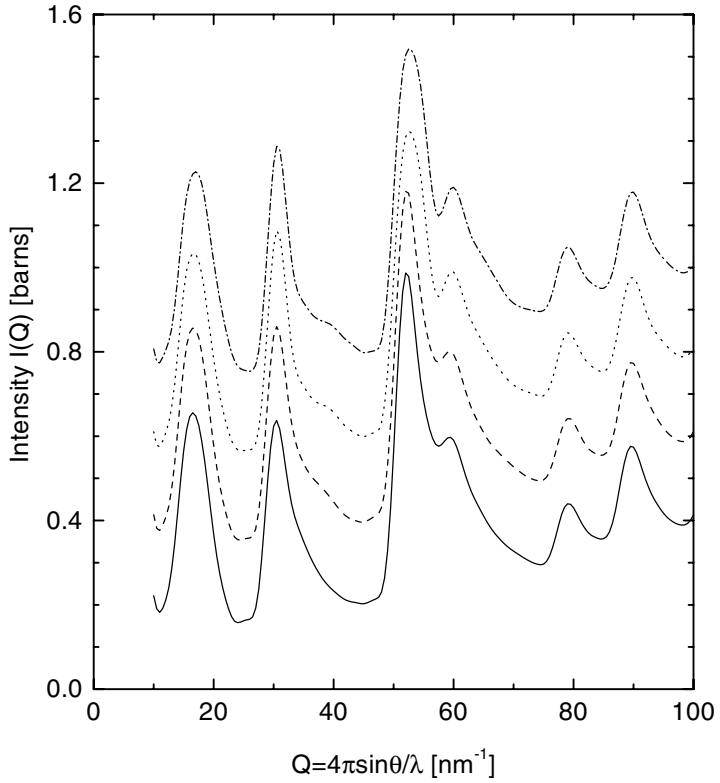

Figure 5. Comparison of four different simulations with random translations from the $(-a/2, a/2)$ (solid line) and $(-a/4, a/4)$ (dashed line) ranges and random rotation angles from the $(-\pi/2, \pi/2)$ (dotted line) and $(-\pi/4, \pi/4)$ (dotted–dashed line) ranges in the Q-range from 0 to 100 nm^{-1}.

Then the paracrystalline structure in the c-axis direction was generated. The one-dimensional paracrystalline lattice was generated by successive translation vectors having Gaussian distribution with the standard deviation σ and the mean value d as the adjustable parameters. In the present calculations the Gaussian distribution of the interplanar spacing with the mean value of 0.345 nm and the standard deviation σ_1 of 0.025 nm were used. In order to obtain a good statistical representation of the normal distribution it was necessary to calculate the intensity function many times and then to take the arithmetic average. The simulation based on the central-limit theorem which gives a series of random numbers with

the Gaussian distribution was used [16] as described in section 2. After 200 simulations the stable intensity functions were obtained. The results of such a simulation, based on the turbostratic structure with paracrystalline stacking of layers, are shown in figure 6. Both peak positions and amplitudes are precisely reproduced by the model constructed in the range of Q from 0 to 250 nm^{-1}. The model function matches the experimental intensity; however, a small phase difference between the experimental and calculated functions remains for larger Q-values (from 250 nm^{-1} to 500 nm^{-1}). All model peaks are slightly shifted towards smaller Q-values. In order to test the model by analysis in real space, the reduced RDF was computed according to equation (3). The $d(r)$ function obtained is compared with the experimental data in figure 7. From the comparison of the curves shown in figure 7 it can be concluded that this model does not explain the structure within the first coordination shell very well, because the small peak observed in the experimental $d(r)$ function at about 0.154 nm is not reproduced by the simulation.

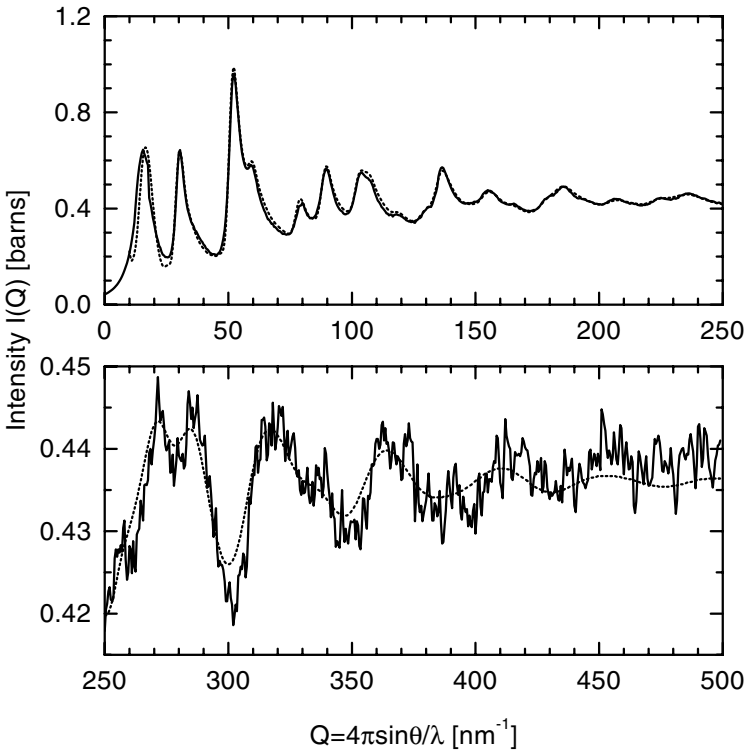

Figure 6. Experimental intensity functions (solid line) and intensity functions calculated with the turbostratic model with random layer translations from the $(-a/2, a/2)$ range (dotted line) in the 0–250 nm^{-1} and 250–500 nm^{-1} ranges.

The occurrence of the small peak at about 0.154 nm in the reduced RDF can be explained by referring to the concept of the quinoid structure [11]. This kind of structure was proposed by Pauling [10]. The quinoid hypothesis is based on the assumption that each carbon atom forms one double (shorter) and two single (longer) bonds. In hexagonal graphite the double bond is assumed to resonate equally among the three positions leading to ideal hexagonal symmetry. The quinoid structure is not a completely resonating structure and it and the graphite structure can be regarded as extreme cases. Ergun and Schehl [9] and Mildner and Carpenter [7] have

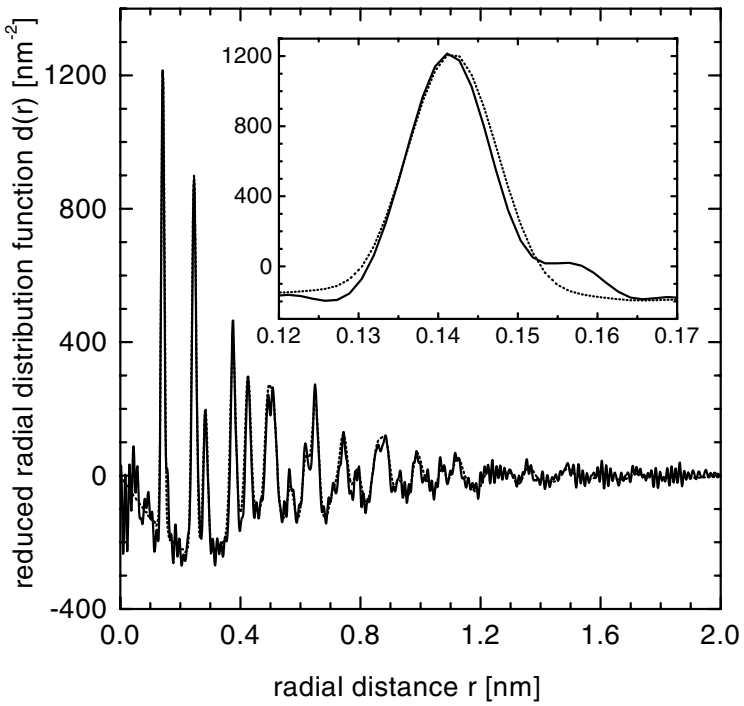

Figure 7. Experimental (solid line) and calculated (dotted line) $d(r)$ functions, for the one-shell model of the first coordination sphere.

considered four structures of a graphite layer as possible variants of the disordered carbon model. These authors have shown that the experimental RDF, obtained from the x-ray and reactor neutron scattering experiments, can be reproduced by disordered quinoid models; however, the first RDF peak was not split because of a much lower $Q_{\max}$-value.

In the present study the quinoidal distortion of the structure was introduced into the model by splitting the near-neighbour interatomic distance into the two distances of 0.140 nm and 0.154 nm. The values of the two near-neighbour distances were adjusted and their weights for each distance were evaluated taking the coordination numbers obtained by the two-shell fit to the first coordination sphere [11]. The RDF peak positions r, the coordination numbers N and the standard deviations of the interatomic distances σ are: $r_1 = 0.140$ (± 0.001) nm, $N_1 = 2.41$ (± 0.25), $\sigma_1 = 0.004$ (± 0.001); $r_2 = 0.154$ (± 0.001) nm, $N_2 = 0.41$ (± 0.25), $\sigma_2 = 0.005$ (± 0.001). Then the $I(Q)$ function was calculated assuming two near-neighbour interatomic distances using the same programs. The experimental and simulated curves are compared in figure 8. This comparison shows that the agreement between the experimental and simulated $I(Q)$ functions is better than that for the one-shell model of the first coordination sphere, especially in the high-Q range where both functions are in phase. It is noteworthy that the quinoid model also improves the agreement between the experimental and calculated $d(r)$ functions. This model reproduces the small peak in the $d(r)$ function in the vicinity of the large peak at 0.141 nm. This is a consequence of a good agreement between the experimental observation and the simulation in the 250–500 nm^{-1} Q-range. The reduced RDF functions, experimental and calculated with the model based on the turbostratic and quinoid structure, are shown in figure 9.

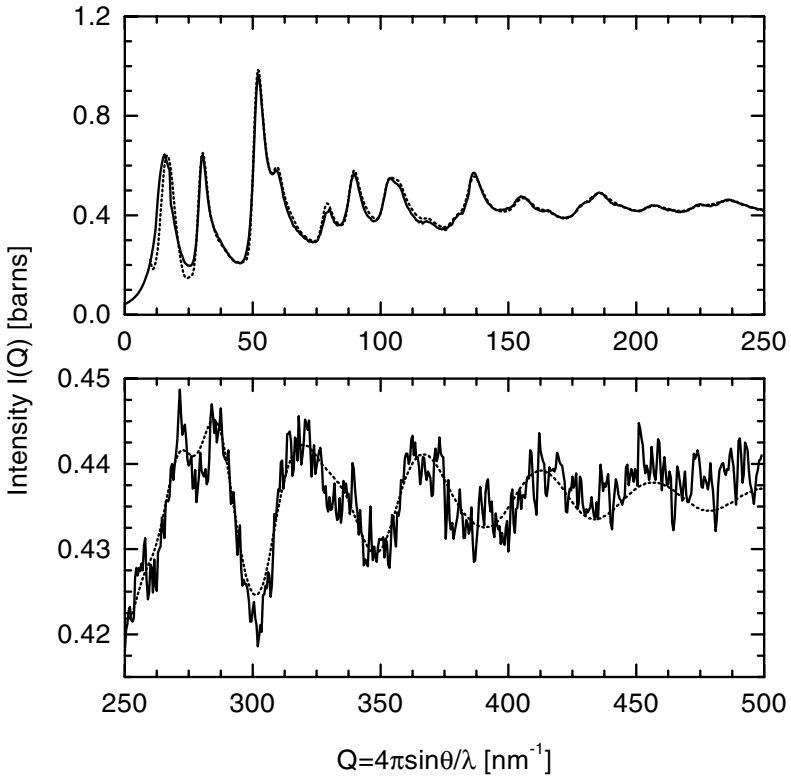

Figure 8. Experimental intensity functions (solid line) and intensity functions calculated with the turbostratic and quinoid model (dotted line) in the 0–250 nm^{-1} and 250–500 nm^{-1} ranges.

3.2. The high-Q fitting procedure

Additional attempts were made to fit the experimental function in the high-Q region using the non-linear least-squares procedure based on the Marquardt–Levenberg algorithm in which r_i, N_i and σ_i are allowed to vary [20]. It was necessary to smooth the experimental intensity function before fitting because the raw intensity data were very noisy in the high-Q range and the fitting procedure was unstable. The three-point Golay–Savitsky method was used in the present work [21]. It was found that the fitting procedures converged when four- and six-parameter sets (r_i, N_i and σ_i) were taken for computation in the Q-ranges 300–500 nm^{-1} and 250–500 nm^{-1}, respectively. The appropriate choice of the number of coordination spheres (or fitting parameters) is the crucial point of the fitting method. At the beginning it is necessary to test this number carefully by a process of trial and error in order to establish a minimal number of free parameters for a given Q-range. We have found that four and six coordination spheres give the main contributions to the intensity in the 300–500 nm^{-1} and 250–500 nm^{-1} Q-ranges, respectively.

The interatomic distances and the coordination numbers of graphite with the quinoid splitting of the first coordination sphere were taken as the starting parameters. The values of these parameters are collected in table 1. The results of such a fitting are compared with the smoothed experimental intensities in figure 10. The structural parameters obtained from the fitting procedure are listed in table 1 together with the values of the starting parameters. The

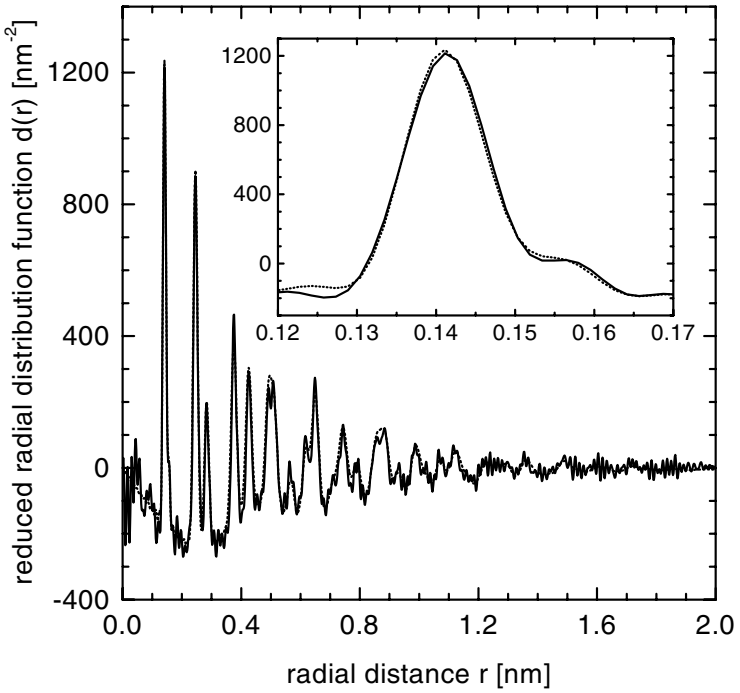

Figure 9. Experimental (solid line) and calculated (dotted line) $d(r)$ functions, for the two-shell model of the first coordination sphere.

Table 1. The results of the fitting procedure together with the starting parameters. The estimated uncertainties are given in parentheses. r indicates the interatomic distance, σ is the standard deviation of the interatomic distance and N is the coordination number.

Starting parameters			Six-parameter sets			Four-parameter sets		
r (nm)	N	σ (nm)	r (nm)	N	σ (nm)	r (nm)	N	σ (nm)
0.141	2.5	0.005	0.141 (0.002)	2.54 (0.25)	0.004 (0.001)	0.140 (0.002)	2.68 (0.25)	0.005 (0.001)
0.154	0.5	0.005	0.155 (0.002)	0.30 (0.25)	0.005 (0.001)	0.154 (0.002)	0.19 (0.25)	0.005 (0.001)
0.244	6	0.007	0.245 (0.002)	5.81 (0.50)	0.006 (0.002)	0.244 (0.002)	7.04 (0.50)	0.006 (0.002)
0.282	3	0.008	0.280 (0.002)	4.22 (1.00)	0.007 (0.002)	0.280 (0.002)	2.42 (1.00)	0.007 (0.002)
0.375	6	0.01	0.373 (0.005)	8.29 (2.00)	0.008 (0.002)	—	—	—
0.425	6	0.01	0.426 (0.005)	6.64 (2.00)	0.009 (0.002)	—	—	—

discrepancy factor R calculated as

$$R = \left\{ \sum_i [I_{\exp}(Q_i) - I_{cal}(Q_i)]^2 \Big/ \sum_i I_{\exp}(Q_i)^2 \right\}^{1/2} \tag{7}$$

is about 2%. The interatomic distances r, their standard deviations σ and the coordination numbers for the first coordination sphere are very close to these derived from an analysis of the data in real space [11] and to the parameters of the model proposed in this paper. Larger discrepancies are observed for the third-neighbour coordination numbers. These differences can be explained by the relatively small interatomic distances within the 0.245 nm and 0.280 nm

coordination spheres. The fitting procedure cannot separate these two contributions precisely, as they contribute to the scattered intensity with similar frequencies. The remaining parameters agree well with the results shown in table 1 in our previous paper [11]. Comparison of the experimental and computed curves for the best-fit parameters shows that the agreement between them is good. All features of the experimental intensities (amplitudes and frequencies) can be reproduced satisfactorily by the model based on the graphite-like structure with paracrystalline distortions of the lattice resulting from the random distribution of the quinoid elements. It is essential to point out that an increase in the σ-value has also been found by using the curve-fitting procedure in reciprocal space which is an indication of the paracrystalline nature of the lattice distortion.

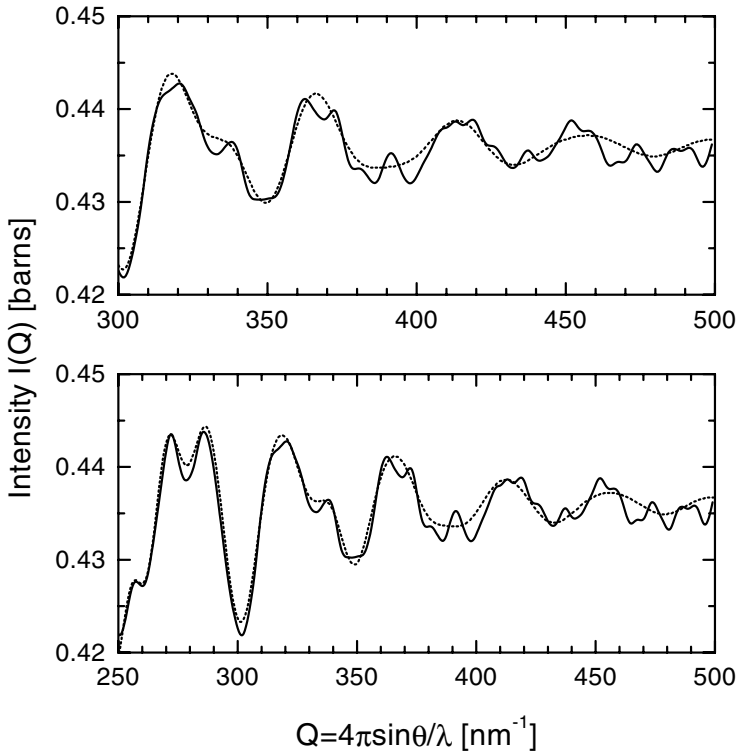

Figure 10. Comparison of smoothed experimental (solid line) and best-fit (dotted line) intensity functions—the four-parameter fit in the Q-range from 300 nm^{-1} to 500 nm^{-1} and the six-parameter fit in the Q-range from 250 nm^{-1} to 500 nm^{-1}.

4. Discussion

The intensity functions for the samples with 0%, 14% and 32% 'burn-off' are very similar above the Q-value of 20 nm^{-1}. This suggests that the local structure within a single layer is not affected by the 'burn-off' process. The same conclusion was also reached by Gardner *et al* for carbons prepared from olive stones [22]. It is well known that an activation process leads to the creation of the different size pores in carbon materials [1]. Taking into account that the degree of 'burn-off' has a practically unobservable effect on the intensity over a wide-Q range, the question arises of how the structure of the carbons investigated is modified

during the activation process. The present results suggest that the ordered regions remain practically unchanged within the precision of the method and that probably the atoms lying within cross-links between ordered regions are removed because the structure of the cross-links is expected to be less ordered and the contribution coming from the cross-links should be much weaker.

We use the paracrystalline concept to obtain a better fit to the experimental intensities. The paracrystalline nature of the two-dimensional network (within a single atomic layer) is associated with the presence of two bond lengths in the carbons investigated and also causes broadening of the diffraction peaks [11]. Such a network can be simulated by packing atoms of the same size in a regular, two-dimensional hexagonal structure. If a certain number of the atoms are replaced by larger atoms, statistically distributed over the network, the network exhibits paracrystalline disorder as explained in section 2 [14, 15]. For the carbons investigated, the lattice distortion parameter g which has been found to be 0.034–0.038 leads to an average number of net-planes in the paracystal $N = 16$–19. In the planar graphite structure the α^*-relation (equation (4)) is related to the rows of atoms with the highest atomic density (here $\{1\bar{1}\}$) and finally the size of the planar paracrystal is estimated to be 1.9–2.3 nm [15, 16], which is in good agreement with the assumed model size. This model explains also the broadening of the peaks because disorder increases with the interatomic distance r. The occurrence of the small peaks in the $d(r)$ functions of about 0.154 nm can be explained by the concept of the quinoid structure proposed by Pauling [10]. The paracrystalline nature of the two-dimensional network within a single layer can be related to the quinoid model with random distribution such that the longer near-neighbour interatomic distances produce the paracrystalline distortion of the lattice.

In the case of the carbons investigated, the quinoid deformation of the hexagonal structure has an effect on the stacking of the layers. Pauling concluded that the quinoid structure permits better packing of the superimposed layers and a consequent decrease in the interlayer spacing and an increased stabilization of this structure by Van der Waals interaction between adjacent layers. A local decrease in the interplanar spacing is related to the random distribution of the quinoid elements in the hexagonal network and suggests local curvature of the layers. It was also suggested that the distorted quinoid rings are likely to be found in the vicinity of defects because their distortion is less under strain than that of complete resonating rings [9]. This leads to additional stabilization because of the smaller bond angle and the reduced bond-compression strain [10, 23].

From the amplitudes of the $d(r)$ peaks one can conclude that the quinoid structure coexists with that of a single graphite sheet. In the quinoid structure each atom is bonded to its three neighbours by one double and two single bonds. In the observed $d(r)$ functions the peaks at about 0.154 nm are smaller than the main near-neighbour peak at 0.139 nm. Therefore, in the proposed model only an admixture of the longer interatomic distances is assumed. Such conclusions are drawn also from the analysis of the data in reciprocal space.

The presence of a significant proportion of sp^3 bonds is not expected for such prepared carbon materials [24, 25]. It was concluded that the sp^3 bonds are not stable at temperatures above 1300 K and it is reasonable to assume that in the carbons investigated the content of tetrahedrally bonded carbon atoms is practically negligible, if they are present at all. It seems to be of interest to consider whether the presence of non-graphitic elements, e.g. five- or seven-membered rings, can be deduced from the present studies. Harris and Tsang [24], Harris [26] and Harris *et al* [27] suggested the presence of fullerene- and nanotube-like atomic arrangement in non-graphitizing carbons on the basis of the high-resolution electron microscopy observations. On the other hand, the diffraction pattern of the C_{60} fullerene, shown in figures 1 and 2 in [28], differs from those presented in the present paper. The RDF obtained by

Li and co-workers [28] exhibits the near-neighbour peak at 0.144 nm. The authors reproduced this peak assuming double- and single-bond lengths of 0.139 and 0.146 nm, respectively. These values are in good agreement with predictions of *ab initio* molecular dynamics simulations yielding the average lengths of 0.140 and 0.145 nm [29]. In the present work the observed position of the first peak is clearly closer and the single-bond length 0.154 nm is significantly longer than the value found in [28, 29]. Significant differences between the neutron diffraction patterns and the RDFs of carbon nanotubes and activated carbons has been reported in [30]. Therefore, the occurrence of fullerenes and nanotubes in the pure form is not expected in activated carbons. However, the paracrystalline distortion of the hexagonal network can also be produced by random distribution of the five- and seven-membered rings, loading to local curvature of a single graphene sheet. The loss of structural coherence beyond about 2 nm along the graphene sheet is also most probable due to the curvature of sheets and distribution of curvatures in the sample according to suggestions made in [31]. Taking into account these suggestions, the presence of locally curved carbon sheets cannot be completely ruled out, although their occurrence in a significant proportions cannot be directly deduced from the present neutron scattering data.

5. Summary and conclusions

The neutron diffraction studies were performed on a series of activated carbons, obtained from a phenolic polymer resin. The pulsed neutron source permitted the diffraction data to be measured for scattering vectors up to 500 nm^{-1}. The structural analysis was made in reciprocal space using Debye's equation with the appropriate Debye–Waller factor to compute the intensity function $I(Q)$. The experimental data recorded using the pulsed neutron facility and the time-of-flight method allowed the experimental intensity to be extended to a high Q-range—much higher than achieved in any other diffraction studies on graphite-like carbons. In the current interpretation method the intensities were calculated on the basis of a model in which the atomic Cartesian coordinates were taken to obtain the interatomic distances in the Debye equation. This approach differs from that proposed by Warren and Kodera and by Minami and Ino who used analytical formulae [4–6]. The curve-fitting method can be applied for a high Q-range yielding reliable structural parameters for the interatomic distances, their standard deviations and the coordination numbers for 4–6 coordination spheres. The structure of activated carbons is based on the disordered graphite-like model with very weak interlayer spatial correlations. Modelling studies have shown that a model consisting of 3–4 layers each about 2 nm in diameter accounts very well for the experimental data.

In order to reproduce the observed decrease in intensity and broadening of the diffraction lines, the Debye–Waller factor, $\exp(-Q^2\sigma^2/2)$ with $\sigma = \sigma_0\sqrt{r}$, was introduced. This form of the attenuation factor is predicted by the paracrystalline theory based on the law of propagation of disorder in such lattices. The results support the turbostratic structure in all samples investigated, with paracrystalline structure along the c-axis. The paracrystalline structure within a single layer and in the layer stacking is related to the presence of quinoid elements. These findings are in agreement with the analysis of the experimental data in real space performed previously [11], but more precise information about the range of ordering along the c-axis can be deduced from the present analysis.

It is essential to point out that the simulation method developed, which uses the Cartesian coordinates of the atoms in the model, could also be used in the case of any model for which the Cartesian coordinates are known, such as those of fullerenes or nanotubes, in both single- and multi-walled forms.

Acknowledgments

We thank Dr D Cazorla-Amoros of the Department of Inorganic Chemistry, University of Alicante, for providing the samples and Mgr M Śliwiński of the University of Silesia for participation in the experiment and the data processing. Beam-time for this experiment on the ISIS facility was supported by the neutron programme of the EPSRC. AS and AB wish to acknowledge the State Committee for Scientific Research for financial support (KBN grant No 5PO3 B03320).

References

[1] Bansal R C, Donnet J-B and Stoeckli F 1988 *Active Carbon* (New York: Dekker)
[2] Klinik J and Grzybek T 1992 *Fuel* **71** 1303
[3] Molina-Sabio M, Perez V and Rodriguez-Reinoso F 1994 *Carbon* **32** 1259
[4] Warren B E 1941 *Phys. Rev.* **9** 693
[5] Warren B E and Bodenstein P 1965 *Acta Crystallogr.* **18** 282
[6] Kodera S, Minami N and Ino T 1986 *Japan. J. Appl. Phys.* **25** 3
[7] Mildner D F R and Carpenter J M 1973 *Proc. 5th Int. Conf. on Amorphous and Liquid Semiconductors (Garmisch-Partenkirchen)* vol 1, ed J Stuce and W Brening, p 463
[8] Alvarez M C and Dore J C 1996 unpublished
[9] Ergun S and Schehl R 1973 *Carbon* **11** 127
[10] Pauling L 1966 *Proc. Natl Acad. Sci. USA* **56** 1646
[11] Burian A, Ratuszna A, Dore J C and Howells W S 1998 *Carbon* **36** 1613
[12] Dore J C, Śliwiński M, Burian A, Howells W S and Cazorla-Amoros D 1999 *J. Phys.: Condens. Matter* **11** 9189
[13] Mitchell G R 1981 *Acta Crystallogr.* A **37** 488
[14] Hosemann R and Bagchi S N 1962 *Direct Analysis of Diffraction by Matter* (Amsterdam: North-Holland) p 69
[15] Hindeleh A M and Hosemann R 1988 *J. Phys. C: Solid State Phys.* **21** 4155
[16] Hosemann R and Hindeleh A M 1995 *J. Macromol. Sci.—Phys.* B **34** 327
[17] Martin B R 1971 *Statistics for the Physicist* (London: University College London Press) pp 26, 47–9
[18] Soper A K, Howells W S and Hannon A C 1989 ATLAS (analysis of time-of-flight diffraction data from liquid and amorphous samples *Rutherford Appleton Laboratory Report*
[19] Noda T, Inagaki M, and Yamada S 1969 *J. Non-Cryst. Solids* **1** 285
[20] Marquardt D W 1963 *J. Soc. Indust. Appl. Math.* **11** 431
[21] Savitzky A and Golay M J E 1964 *Anal. Chem.* **36** 627
[22] Gardner M A, Dore J C, North A N, Cazorla-Amoros D, Salinas-Martinez de Lecea C and Bellisent-Funel M C 1996 *Carbon* **34** 857
[23] Rousseaux F and Tchoubar D 1977 *Carbon* **15** 55
[24] Harris P J F and Tsang S C 1997 *Phil. Mag.* A **76** 667
[25] Diaz J, Paolicelli G, Ferrer S and Comin F 1996 *Phys. Rev.* **54** 8064
[26] Harris P J F 1997 *Int. Mater. Rev.* **42** 206
[27] Harris P J F, Burian A and Duber S 2000 *Phil. Mag. Lett.* **80** 381
[28] Ramage F, Li D, Lamin J S and Conceicao J 1992 *Phys. Rev.* B **44** 13 167
[29] Zhang Q M, Yi J Y and Bernholc J 1991 *Phys. Rev. Lett.* **66** 2633
[30] Burian A, Dore J C, Fisher H E and Sloan J 1999 *Phys. Rev.* B **59** 1665
[31] Petkow V, DiFrancesco G and Billinge S J L 1999 *Phil. Mag.* B **79** 1519